

# Constraints on primordial curvature spectrum from primordial black holes and scalar-induced gravitational waves

Zhu Yi<sup>a,1</sup>, Qin Fei<sup>b,2</sup>

<sup>1</sup>Advanced Institute of Natural Sciences, Beijing Normal University, Zhuhai 519087, China

<sup>2</sup>School of Mathematics and Physics, Hubei Polytechnic University, Huangshi 435003, China

Received: date / Accepted: date

**Abstract** The observational data of primordial black holes and scalar-induced gravitational waves can constrain the primordial curvature perturbation at small scales. We parameterize the primordial curvature perturbation by a broken power law form and find that it is consistent with many inflation models that can produce primordial black holes, such as nonminimal derivative coupling inflation, scalar-tensor inflation, Gauss-Bonnet inflation, and K/G inflation. The constraints from primordial black holes on the primordial curvature power spectrum with the broken power law form are obtained, where the fraction of primordial black holes in dark matter is calculated by the peak theory. Both the real-space top-hat and the Gaussian window functions are considered. The constraints on the amplitude of primordial curvature perturbation with Gaussian window function are around three times larger than those with real-space top-hat window function. The constraints on the primordial curvature perturbation from the NANOGrav 12.5yrs data sets are displayed, where the NANOGrav signals are assumed as the scalar-induced gravitational waves, and only the first five frequency bins are used.

## 1 Introduction

Primordial black holes (PBHs) are formed from the overdense regions of the Universe by gravitational collapse during radiation domination [1, 2]. They can explain the source of the gravitational waves (GWs) events detected by the Laser Interferometer Gravitational Wave Observatory (LIGO) Scientific Collaboration and the Virgo Collaboration [3–17]. They are also dark matter (DM) candidates [18–27] due to the non detection of particle dark matter. For the PBHs with masses around  $10^{-17} - 10^{-15}M_{\odot}$  and  $10^{-14} - 10^{-12}M_{\odot}$ , they

can make up almost all dark matter because of no observational constraints on the abundances of PBHs at these two mass windows. The seed of the overdense regions that collapse to form PBHs can come from the primordial curvature perturbations generated during inflation [28–31]. To produce enough PBHs DM, the amplitude of the power spectrum of the primordial curvature perturbations should be around  $A_{\zeta} \sim \mathcal{O}(0.01)$ . From the observation of cosmic microwave background (CMB) anisotropy measurements, the constraints on the primordial curvature perturbations are  $A_{\zeta} = 2.1 \times 10^{-9}$  [32] at large scales,  $k \lesssim \mathcal{O}(1)\text{Mpc}^{-1}$ . Therefore, to produce enough PBHs DM, the primordial curvature power spectrum should be enhanced by about seven orders of magnitude at small scales, compared with the constraints at larger scales [33].

The amplitude of the primordial curvature perturbations can be sharply enhanced if there is an ultra-slow-roll phase in the inflation model [34–36]. For the single field inflation models, the ultra-slow-roll phase can be realized by the canonical inflation models with an inflection point [33, 37–44], and the ultra-slow-roll phase can also be realized by many noncanonical inflation models [45–64]. The speed of the enhancement of the primordial curvature perturbations of the single field inflation can not be arbitrarily fast; the steepest enhancement obeys the power law form,  $\mathcal{P}_{\zeta} \sim k^4$  [65, 66]. Guided by this property, the typical peaks in the power spectrum of the primordial curvature perturbations generated by single field inflation can be approximated by a broken power law,  $\mathcal{P}_{peak}(k) = A(\alpha + \beta)/[\beta(k/k_p)^{-\alpha} + \alpha(k/k_p)^{\beta}]$  [67]. Considering the large scales constraints, the power spectrum of the primordial curvature perturbations can be approximated by  $\mathcal{P}_{\zeta}(k) = A(\alpha + \beta)/[\beta(k/k_p)^{-\alpha} + \alpha(k/k_p)^{\beta}] + A_*(k/k_*)^{n_{*s}-1}$ . In this paper, we show that the broken power law form of the primordial curvature perturbation is consistent with many inflation models such as the

<sup>a</sup>e-mail: yz@bnu.edu.cn

<sup>b</sup>e-mail: feiqin@hbpu.edu.cn

inflation model with nonminimal derivative coupling [46], scalar-tensor inflation model [59], Gauss-Bonnet inflation model [60], and inflation model with non-canonical kinetic term (K/G inflation) [57].

The observational data of PBHs can provide constraints on the primordial curvature perturbations at small scales. There are many works on this topic. The constraints on the primordial curvature perturbations from the PBHs observational data with Press-Schechter theory and Gaussian window function are discussed in ref. [68]. The constraints considering all the steps from gravitational collapse to PBHs formation in real space are obtained in ref. [69]. And the constraints with peak theory are given in ref. [70] where the power spectrum of the primordial curvature perturbation is chosen as the log-normal form. As the broken power law form of the primordial curvature perturbation are consistent with many inflation models, in this paper, we use the broken power law form and give the constraints on primordial curvature perturbation from the observational data of PBHs with peak theory. Both Gaussian and real-space top-hat window functions are considered.

Accompanying the formation of PBHs, the large scalar perturbations can induce secondary gravitational waves after the horizon reentry during the radiation-dominated epoch [71–105]. The scalar-induced gravitational waves (SIGWs), containing much information about the early Universe, have wide frequency distribution and can be detected by pulsar timing arrays (PTA) [106–110] and the future space-based GW detectors such as Laser Interferometer Space Antenna (LISA) [111, 112], Taiji [113], and TianQin [114]. The stochastic process with a common amplitude and a common spectral slope across pulsars detected by the North American Nanohertz Observatory for Gravitational Wave (NANOGrav) Collaboration [115] and other pulsar timing arrays [116, 117] can be explained by SIGWs [58, 67, 118–120]. In this paper, we give the constraints on the primordial curvature perturbation from the NANOGrav 12.5yrs data sets by regarding the NANOGrav signals as GWs induced from the primordial curvature perturbation with the broken power law form.

This paper is organized as follows. In Sec. 2, we calculate the abundance of PBHs from the power spectrum of primordial curvature perturbation by peak theory. In Sec. 3, we give the energy density of SIGWs. We discuss the constraints from the PBHs and SIGWs on the power spectrum of primordial curvature perturbation in Sec. 4. We conclude the paper in Sec. 5.

## 2 The primordial black holes

The fraction of the Universe in PBHs at the formation is denoted by

$$\beta = \frac{\rho_{\text{PBH}}}{\rho_b}, \quad (1)$$

where  $\rho_{\text{PBH}}$  is the energy density of PBHs and  $\rho_b$  is the background energy density of the Universe. From the peak theory, the energy density of PBHs is [70, 121–125]

$$\rho_{\text{PBH}} = \int_{v_c}^{\infty} M_{\text{PBH}}(v) \mathcal{N}_{pk}(v) dv, \quad (2)$$

where  $v = \delta/\sigma$  and  $v_c = \delta_c/\sigma_0$ ,  $\delta_c$  is the threshold of the smoothed density contrast for the formation of PBHs and  $\sigma_0$  is the variance of the smoothed density contrast.  $M_{\text{PBH}}$  is the mass of PBHs and  $\mathcal{N}_{pk}$  is the number density of PBHs [121],

$$\mathcal{N}_{pk}(v) = \frac{1}{a^3} \frac{1}{(2\pi)^2} \left( \frac{\sigma_1}{\sqrt{3}\sigma_0} \right)^3 v^3 \exp\left(-\frac{v^2}{2}\right). \quad (3)$$

The moment of the smoothed density power spectrum  $\sigma_n$  is defined by

$$\sigma_n^2 = \int_0^{\infty} \frac{dk}{k} k^{2n} T^2(k, R_H) W^2(k, R_H) \mathcal{P}_{\delta}(k), \quad (4)$$

where  $\sigma_0$  and  $\sigma_1$  are obtained by choosing  $n = 0$  and  $n = 1$ , respectively. The power spectrum of the density contrast  $\mathcal{P}_{\delta}$  is related to the power spectrum of primordial curvature perturbations  $\mathcal{P}_{\zeta}$  by

$$\mathcal{P}_{\delta}(k) = \frac{4(1+w)^2}{(5+3w)^2} \left( \frac{k}{aH} \right)^4 \mathcal{P}_{\zeta}(k), \quad (5)$$

where the state equation  $w = 1/3$  during the radiation domination. The most considered window functions  $W(k, R_H)$  in equation (4) are the real-space top-hat window function [126],

$$W(k, R_H) = 3 \left[ \frac{\sin(kR_H) - (kR_H) \cos(kR_H)}{(kR_H)^3} \right], \quad (6)$$

and the Gaussian window function

$$W(k, R_H) = \exp\left(\frac{-k^2 R_H^2}{2}\right), \quad (7)$$

with the smoothed scale  $R_H \sim 1/aH$ . In this paper, both these two window functions are considered. The transfer function in equation (4) is

$$T(k, R_H) = 3 \left[ \frac{\sin\left(\frac{kR_H}{\sqrt{3}}\right) - \left(\frac{kR_H}{\sqrt{3}}\right) \cos\left(\frac{kR_H}{\sqrt{3}}\right)}{(kR_H/\sqrt{3})^3} \right]. \quad (8)$$

The mass of primordial black holes in equation (2) obeys the critical scaling law [127–129],

$$M_{\text{PBH}} = \kappa M_H (\delta - \delta_c)^{\gamma}, \quad (9)$$

where  $\gamma = 0.36$  in the radiation domination [127, 128] and  $M_H$  is the mass in the horizon,

$$M_H \approx 13 \left( \frac{g_*}{106.75} \right)^{-1/6} \left( \frac{k}{10^6 \text{Mpc}^{-1}} \right)^{-2} M_{\odot}, \quad (10)$$

$g_*$  is the number of relativistic degrees of freedom at the formation of PBHs. The parameter  $\kappa$  in the critical scaling law and PBHs formation threshold  $\delta_c$  are dependent on the window function, and the relations of them between the two window functions are [125]

$$\delta_{c(G)} \approx \frac{\delta_{c(TH)}}{2.17}, \quad \kappa_G \approx \frac{2.74^2 \times 2.17^\gamma}{4} \kappa_{TH}, \quad (11)$$

where  $\gamma$  is the index in the critical scaling law (9). For the real-space top-hat window function, we choose  $\delta_{c(TH)} = 0.51$  and  $\kappa_{TH} = 3.3$  [130, 131]; from equation (11), the corresponding values for the Gaussian window function are  $\delta_{c(G)} \approx 0.24$  and  $\kappa_G = 8.2$ .

Combining the mass fraction of the Universe which collapses to form PBHs, equation (1), with the background equation of the energy density of the Universe, we obtain the density parameter of PBHs at present [132],

$$\Omega_{\text{PBH}} = \int_{M_{\text{min}}}^{M_{\text{max}}} d \ln M_H \left( \frac{M_{\text{eq}}}{M_H} \right)^{1/2} \beta(M_H), \quad (12)$$

where we use the relations  $\rho_{\text{PBH}} \propto a^{-3}$  and  $\rho_b \propto a^{-n}$ , with  $n = 4$  during radiation domination and  $n = 3$  during matter domination; and  $M_{\text{eq}} = 2.8 \times 10^{17} M_\odot$  is the horizon mass at the matter-radiation equality. The limits of the integral are taken as  $M_{\text{min}} = 0$  and  $M_{\text{max}} = \infty$  because of  $\beta(M_H) \rightarrow 0$  at the condition  $M_H \rightarrow 0$  or  $M_H \rightarrow \infty$ . The fraction of primordial black holes in the dark matter at present is defined as

$$f_{\text{PBH}} = \frac{\Omega_{\text{PBH}}}{\Omega_{\text{DM}}} = \int f(M_{\text{PBH}}) d \ln M_{\text{PBH}}, \quad (13)$$

where  $\Omega_{\text{DM}}$  is the density parameter for dark matter, and the PBHs mass function is

$$f(M_{\text{PBH}}) = \frac{1}{\Omega_{\text{DM}}} \frac{d\Omega_{\text{PBH}}}{d \ln M_{\text{PBH}}}. \quad (14)$$

Substituting equation (12) into definition (14) and combining the above equations, we can obtain the PBHs mass function [132],

$$\begin{aligned} f(M_{\text{PBH}}) &= \frac{1}{\Omega_{\text{DM}}} \int_{M_{\text{min}}}^{M_{\text{max}}} \frac{dM_H}{M_H} \frac{M_{\text{PBH}}}{\gamma M_H} \sqrt{\frac{M_{\text{eq}}}{M_H}} \\ &\times \frac{1}{3\pi} \left( \frac{\sigma_1}{\sqrt{3}\sigma_0 a H} \right)^3 \frac{1}{\sigma_0^4} \left( \mu^{1/\gamma} + \delta_c \right)^3 \\ &\times \mu^{1/\gamma} \exp \left[ -\frac{(\mu^{1/\gamma} + \delta_c)^2}{2\sigma_0^2} \right], \end{aligned} \quad (15)$$

where  $\mu = M_{\text{PBH}}/(\kappa M_H)$  and the relation  $d\delta/d \ln M_{\text{PBH}} = \mu^{1/\gamma}/\gamma$  derived from equation (9) is used.

### 3 The scalar-induced gravitational waves

Accompanying the formation of PBHs, the large scalar perturbation can induce secondary gravitational waves during the radiation domination. The metric with perturbation in the cosmological background and Newtonian gauge is

$$\begin{aligned} ds^2 &= -a^2(\eta)(1 + 2\Phi)d\eta^2 \\ &+ a^2(\eta) \left[ (1 - 2\Phi)\delta_{ij} + \frac{1}{2}h_{ij} \right] dx^i dx^j, \end{aligned} \quad (16)$$

where the anisotropic stress is neglected,  $\eta$  is the conformal time,  $\Phi$  is the Bardeen potential, and  $h_{ij}$  are the tensor perturbations. The tensor perturbations in the Fourier space can be obtained by the transform

$$h_{ij}(\mathbf{x}, \eta) = \int \frac{d^3 k e^{i\mathbf{k}\cdot\mathbf{x}}}{(2\pi)^{3/2}} [h_{\mathbf{k}}(\eta)e_{ij}(\mathbf{k}) + \tilde{h}_{\mathbf{k}}(\eta)\tilde{e}_{ij}(\mathbf{k})], \quad (17)$$

where  $e_{ij}(\mathbf{k})$  and  $\tilde{e}_{ij}(\mathbf{k})$  are the plus and cross polarization tensors,

$$e_{ij}(\mathbf{k}) = \frac{1}{\sqrt{2}} [e_i(\mathbf{k})e_j(\mathbf{k}) - \tilde{e}_i(\mathbf{k})\tilde{e}_j(\mathbf{k})], \quad (18)$$

$$\tilde{e}_{ij}(\mathbf{k}) = \frac{1}{\sqrt{2}} [e_i(\mathbf{k})\tilde{e}_j(\mathbf{k}) + \tilde{e}_i(\mathbf{k})e_j(\mathbf{k})], \quad (19)$$

with the basis vectors satisfying  $\mathbf{e} \cdot \tilde{\mathbf{e}} = \mathbf{e} \cdot \mathbf{k} = \tilde{\mathbf{e}} \cdot \mathbf{k}$ .

The tensor perturbations in the Fourier space with either polarization induced by the second order of the linear scalar perturbations satisfy [73, 74]

$$h''_{\mathbf{k}} + 2\mathcal{H}h'_{\mathbf{k}} + k^2 h_{\mathbf{k}} = 4S_{\mathbf{k}}, \quad (20)$$

where a prime denotes the derivative with respect to the conformal time  $\eta$ ,  $h'_{\mathbf{k}} = dh_{\mathbf{k}}/d\eta$ , and  $\mathcal{H} = a'/a$  is the conformal Hubble parameter. The second order source from the linear scalar perturbations  $S_{\mathbf{k}}$  is

$$\begin{aligned} S_{\mathbf{k}} &= \int \frac{d^3 \tilde{\mathbf{k}}}{(2\pi)^{3/2}} e_{ij}(\mathbf{k}) \tilde{k}^i \tilde{k}^j \left[ 2\Phi_{\tilde{\mathbf{k}}} \Phi_{\mathbf{k}-\tilde{\mathbf{k}}} + \right. \\ &\left. \frac{1}{\mathcal{H}^2} \left( \Phi'_{\tilde{\mathbf{k}}} + \mathcal{H} \Phi_{\tilde{\mathbf{k}}} \right) \left( \Phi'_{\mathbf{k}-\tilde{\mathbf{k}}} + \mathcal{H} \Phi_{\mathbf{k}-\tilde{\mathbf{k}}} \right) \right], \end{aligned} \quad (21)$$

where  $\Phi_{\mathbf{k}}$  is the Bardeen potential in the Fourier space and can be related to the primordial curvature perturbations  $\zeta_{\mathbf{k}}$  generated in the inflation by the transfer function

$$\Phi_{\mathbf{k}} = \frac{3+3w}{5+3w} T(k, \eta) \zeta_{\mathbf{k}}, \quad (22)$$

where  $T(k, \eta)$  is the transfer function (8).

To solve the tensor perturbations equation (20), the Green function method is used, and the solution is

$$h_{\mathbf{k}}(\eta) = \frac{4}{a(\eta)} \int_{\eta_k}^{\eta} d\tilde{\eta} g_{\mathbf{k}}(\eta, \tilde{\eta}) a(\tilde{\eta}) S_{\mathbf{k}}(\tilde{\eta}), \quad (23)$$

where the corresponding Green function is

$$g_k(\eta, \eta') = \frac{\sin[k(\eta - \eta')]}{k}. \quad (24)$$

Substituting the solution of  $h_k$  (23) into the definition of the power spectrum of tensor perturbations,

$$\langle h_{\mathbf{k}}(\eta) h_{\tilde{\mathbf{k}}}(\eta) \rangle = \frac{2\pi^2}{k^3} \delta^{(3)}(\mathbf{k} + \tilde{\mathbf{k}}) \mathcal{P}_h(k, \eta), \quad (25)$$

we can obtain [73, 74, 88, 89, 133]

$$\begin{aligned} \mathcal{P}_h(k, \eta) = & 4 \int_0^\infty dv \int_{|1-v|}^{1+v} du \left[ \frac{4v^2 - (1 - u^2 + v^2)^2}{4uv} \right]^2 \\ & \times I_{\text{RD}}^2(u, v, x) \mathcal{P}_\zeta(kv) \mathcal{P}_\zeta(ku), \end{aligned} \quad (26)$$

where  $u = |\mathbf{k} - \tilde{\mathbf{k}}|/k$ ,  $v = \tilde{k}/k$ ,  $x = k\eta$ , and the integral kernel  $I_{\text{RD}}$  is

$$\begin{aligned} I_{\text{RD}}(u, v, x) = & \int_1^x dy y \sin(x-y) \{ 3T(uy)T(vy) \\ & + y[T(vy)uT'(uy) + vT'(vy)T(uy)] \\ & + y^2 v^2 T'(uy)T'(vy) \}. \end{aligned} \quad (27)$$

The energy density of Gravitational waves is defined as

$$\Omega_{\text{GW}}(k, \eta) = \frac{1}{24} \left( \frac{k}{aH} \right)^2 \overline{\mathcal{P}_h(k, \eta)}. \quad (28)$$

Substituting equation (26) into the definition (28), we get [89, 133]

$$\begin{aligned} \Omega_{\text{GW}}(k, \eta) = & \frac{1}{6} \left( \frac{k}{aH} \right)^2 \int_0^\infty dv \int_{|1-v|}^{1+v} du \\ & \times \left[ \frac{4v^2 - (1 - u^2 + v^2)^2}{4uv} \right]^2 \\ & \times I_{\text{RD}}^2(u, v, x) \mathcal{P}_\zeta(kv) \mathcal{P}_\zeta(ku), \end{aligned} \quad (29)$$

where  $\overline{\phantom{x}}$  is the oscillation time average of the integral kernel. The evolution of the energy density of the gravitational waves is the same as that of radiation; with the help of this property, the energy density of the gravitational waves at present can be obtained easily,

$$\Omega_{\text{GW}}(k, \eta_0) = \frac{c_g \Omega_{r,0} \Omega_{\text{GW}}(k, \eta)}{\Omega_r(\eta)}, \quad (30)$$

where  $\Omega_{r,0}$  is the energy density of the radiation at present and  $\Omega_r(\eta) = 1$  at the generation of SIGWs, and [67, 118]

$$c_g = 0.387 \left( \frac{g_{*,s}^4 g_*^{-3}}{106.75} \right)^{-1/3}. \quad (31)$$

## 4 The constraints on the primordial power spectrum

At large scales, the constraints on the primordial curvature perturbations from the observation of CMB anisotropy measurements are strong,  $A_\zeta = 2.1 \times 10^{-9}$  [32]. At the same time, there are few constraints on the primordial curvature perturbations at small scales. Because PBHs and scalar-induced GWs are produced from the primordial curvature perturbations with large amplitude at small scales, the successful or failed detection of PBHs and SIGWs can provide constraints on the primordial curvature perturbations at small scales. To produce enough PBHs DM and SIGWs, the power spectrum of the primordial perturbations should be around  $\mathcal{P}_\zeta \sim \mathcal{O}(0.01)$ , which is about seven orders of magnitudes larger than that at large scales. For the single field inflation models, the profile of the enhancement of the power spectrum can be governed by the power law form, and the steepest enhancement is about the order of  $\sim k^4$  [65, 66]. To fit the enhanced primordial power spectrum, we consider the broken power law parameterization [67]

$$\mathcal{P}_\zeta(k) = \frac{A(\alpha + \beta)}{\beta(k/k_p)^{-\alpha} + \alpha(k/k_p)^\beta} + A_*(k/k_*)^{n_{s_*}-1}. \quad (32)$$

The first term is the broken power law form to fit the enhanced peak at small scales,  $0.5 \lesssim \alpha \lesssim 4$  controls the speed of enhancement, and  $0.5 \lesssim \beta \lesssim 4$  determines the speed of decline in the power spectrum. A pair of smaller parameters,  $\alpha$  and  $\beta$ , gives a broader peak in the spectrum. The lower limit of the parameters ensures the curvature power spectrum between the end of inflation and the peak obeys a power law [67]. The second term in equation (32) is the near scale-invariant power law form to fit the Planck 2018 constraints [134] at large scales, and the parameters are chosen as  $k_* = 0.05 \text{Mpc}^{-1}$ ,  $n_{s_*} = 0.965$ , and  $A_* = 2.1 \times 10^{-9}$ .

In figure 1, we compare the parameterization (32) with some real inflation models. The black dashed lines denote the power spectra from real inflation models, and the red solid lines represent the results from parameterization (32). The power spectra in the left upper panel, right upper panel, left lower panel, and right lower panel are from the inflation model with nonminimal derivative coupling [46], scalar-tensor inflation model [59], Gauss-Bonnet inflation model [60], and inflation model with a non-canonical kinetic term (K/G inflation model) [57], respectively. Figure 1 shows that the power spectra from parameterization (32) are consistent well with those from real inflation models both at large and peak scales. The features of PBHs and SIGWs are mainly determined by the high peak region of the power spectrum of the primordial curvature perturbations. Therefore, we can safely use parameterization (32) to research the topic of PBHs and SIGWs.

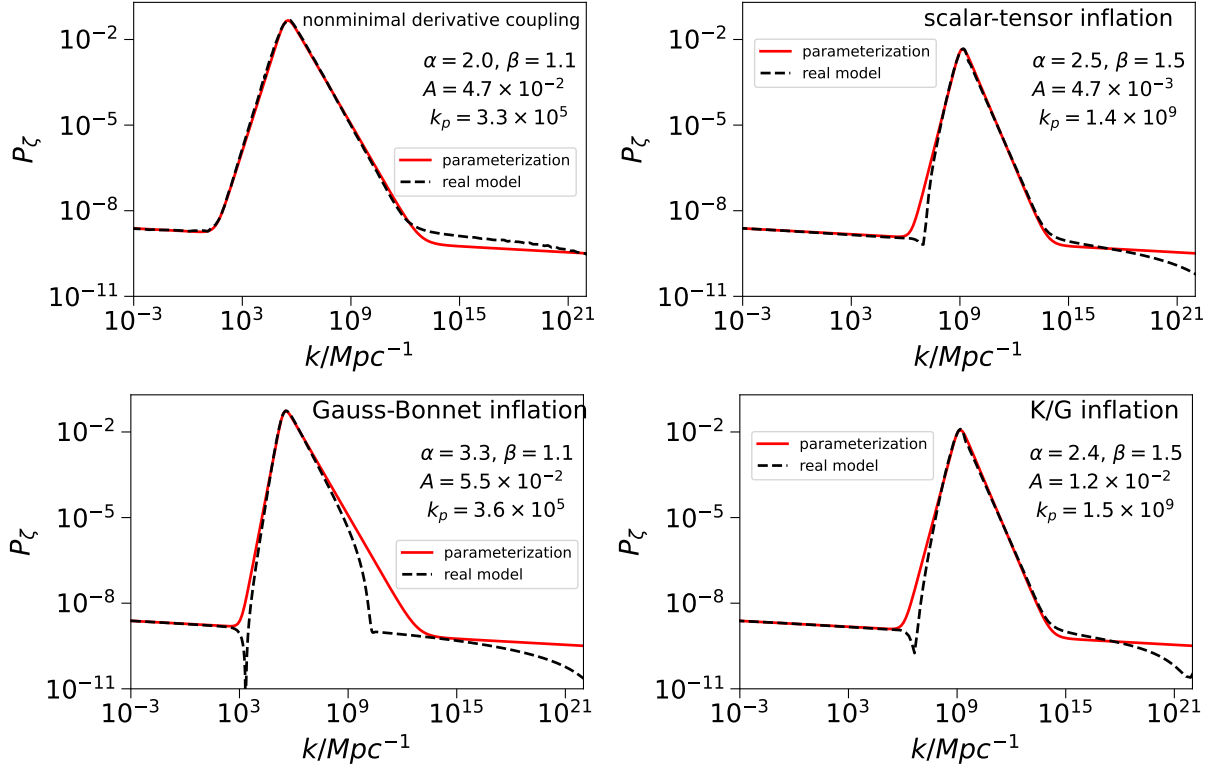


**Fig. 1** The difference between the power spectra from real inflation models (denoted by black dashed lines) and parameterization (32) (marked by solid red lines). The left upper panel, right upper panel, left lower panel, and right lower panel are the power spectra from inflation model with nonminimal derivative coupling [46], scalar-tensor inflation model [59], Gauss-Bonnet inflation model [60], and inflation model with non-canonical kinetic term (K/G inflation) [57], respectively.

#### 4.1 Constraints from PBHs

Combining the parameterization (32) and PBHs mass function (15), we can transfer the constraints on PBHs DM to those on the primordial curvature power spectrum. The left panel of figure 2 shows the main observational data of PBHs DM at present, and the right panel of figure 2 displays the corresponding constraints on the primordial curvature power spectrum from the left panel PBHs DM observational data. In the right panel of figure 2, the red and black bands are the results with the choice of top-hat and Gaussian window functions, respectively. The lower and upper limits of each band are from the parameterization (32) with  $\alpha = \beta = 0.5$  and  $\alpha = \beta = 4$ , respectively. For the choice of the top-hat window function, the constraints on the primordial curvature power spectrum from PBHs DM are more robust than those from BBN and PTA; and for the choice of the Gaussian window function, the constraints are weaker than those from PTA. The uncertainty of the constraints caused by the choice of the window function is more significant than that by the profile of the peak in the primordial curvature power spectrum. The magenta line denotes the constraints from PBHs DM with Press-Schechter theory and Gaussian window function given in ref. [68], and the con-

straints are weaker than that with peak theory. The reason is that the PBHs abundance calculated by the peak theory is larger than that by the Press-Schechter by about one order magnitude for the same primordial power spectrum [122].

Accompanying the PBHs formation, the large scalar perturbations can induce the secondary gravitational waves. Substituting the parameterization (32) into equation (30), we can obtain the energy density of the corresponding SIGWs. According to the lower limits of each band displayed in the right panel of figure 2, we choose the parameter values listed in table 1 to generate SIGWs with peak frequencies around  $10^{-9}$  Hz,  $10^{-3}$  Hz, and  $10^2$  Hz, and the results are shown in figure 3. The labels ‘‘Gauss’’ and ‘‘TopHat’’ in table 1 denote the choices according to the lower limits of the black and red bands in the right panel of figure 2, respectively. The parameter  $f_p$  is the peak frequency of the SIGW. The solid and dashed lines in figure 3 are the energy density of the SIGWs with the parameter value choices labeled as ‘‘TopHat’’ and ‘‘Gauss’’ in table 1, respectively. The green, red, and black lines denote the SIGWs with peak frequencies around  $10^{-9}$  Hz,  $10^{-3}$  Hz, and  $10^2$  Hz, respectively. The SIGWs with  $10^{-9}$  Hz can explain the stochastic common-spectrum process detected by the NANOGrav and other PTA groups recently. In the future, more and more SIGWs with peak fre-

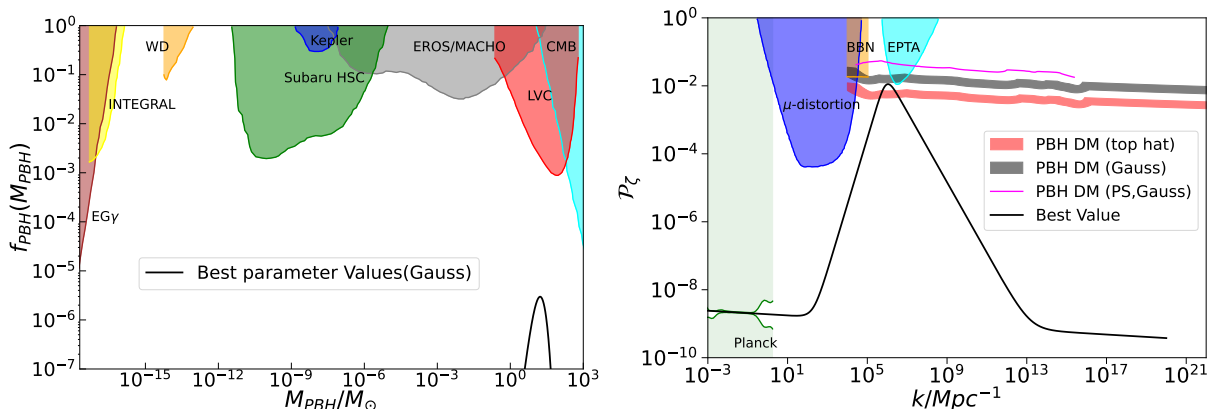


**Fig. 2** The left panel shows the observational constraints on the PBHs abundance: the cyan region from accretion constraints by CMB [135, 136], the red region from LIGO-Virgo Collaboration measurements [137–142], the gray region from the EROS/MACHO [143], the green region from microlensing events with Subaru HSC [144], the blue region from the Kepler satellite [145], the orange region from white dwarf explosion (WD) [146], the yellow region from galactic center 511 keV gamma-ray line (INTEGRAL) [147–149], and the brown region from extragalactic gamma-rays by PBH evaporation ( $EG\gamma$ ) [150]. The right panel shows the constraints on the primordial curvature spectrum. The light green shaded region is excluded by the CMB observations [134]. The cyan, orange and blue regions show the constraints from the EPTA observations [151], the effect on the ratio between neutron and proton during the big bang nucleosynthesis (BBN) [152] and  $\mu$ -distortion of CMB [153], respectively. The red and black bands are from the left panel PBHs observational data. The black curve in the right panel is the parameterization (32) with the best parameter values (33) and (34) obtained from the Bayesian analysis of PTA data, and the black curve in the left panel is the corresponding mass function calculated by the peak theory with the Gaussian window function.

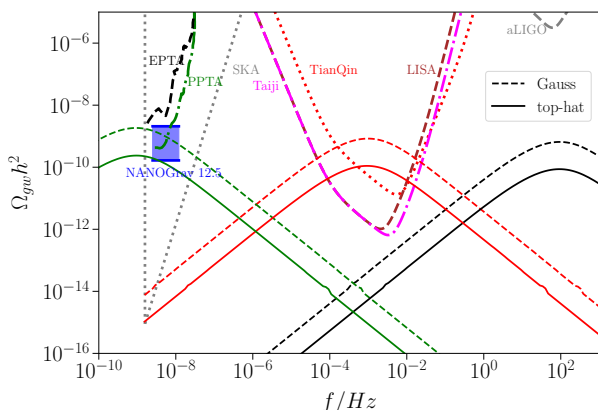


**Fig. 3** The convex curves denote the energy density of SIGWs with peak frequencies around  $10^{-9}$  Hz,  $10^{-3}$  Hz, and  $10^2$  Hz, respectively. The dashed and solid lines are related to the black and red bands in the right panel of figure 2, respectively. The concave curves represent the GWs detectors limits: the black dashed curve denotes the EPTA limit [106–109, 154], the green dot-dashed curve denotes the PPTA limit [155], the gray dotted curve denotes the SKA limit [110], the red dotted curve in the middle denotes the TianQin limit [114], the magenta dot-dashed curve shows the Taiji limit [113], the brown dashed curve shows the LISA limit [112], and the gray dashed curve in the right denotes the aLIGO limit [156, 157].

quency around  $10^{-9}$  Hz may be detected by PTA groups. The SIGWs with  $10^{-3}$  Hz can be detected by the future space-based GWs detectors such as LISA, Taiji, and TianQin. Under the present PBHs DM observational data constraints, the corresponding SIGWs can be detected by both the present PTA and future space-based GW detectors. More information about inflation at small scales will be obtained

Model	A	$k_p$	$f_p/\text{Hz}$
Gauss1	$1.23 \times 10^{-2}$	$6.36 \times 10^5$	$9.83 \times 10^{-10}$
Gauss2	$8.30 \times 10^{-3}$	$6.72 \times 10^{11}$	$1.04 \times 10^{-3}$
Gauss3	$7.34 \times 10^{-3}$	$6.39 \times 10^{16}$	$9.88 \times 10^1$
TopHat1	$4.42 \times 10^{-3}$	$6.51 \times 10^5$	$1.01 \times 10^{-9}$
TopHat2	$3.02 \times 10^{-3}$	$6.37 \times 10^{11}$	$9.84 \times 10^{-4}$
TopHat3	$2.67 \times 10^{-3}$	$6.35 \times 10^{16}$	$9.82 \times 10^1$

**Table 1** The parameter values of the parameterization (32) with  $\alpha = \beta = 0.5$ .

with more observational data about SIGWs being detected. The SIGWs with peak frequencies around  $10^2$  Hz cannot be detected by the aLIGO detector; therefore, the aLIGO detector can tell us little information about the inflation at small scales through SIGWs at present.

#### 4.1.1 Constraints from all dark matter

Due to the failure of direct detection of particle dark matter, it is warranted to consider the possibility of PBHs as a DM candidate. There are no constraints on PBHs DM abundance at the two mass windows  $10^{-17} - 10^{-15} M_\odot$  and  $10^{-14} - 10^{-12} M_\odot$ , as displayed in the left panel of figure 2; therefore, PBHs with masses locating at these two windows can make up all the dark matter. Combining the parameterization (32) and PBHs mass function (15), we can obtain the constraints on the primordial power spectrum if the PBHs DM make up all the dark matter, and the results are shown in figure 4, where the peak scale  $k_p$  in parameterization (32) is chosen as  $k_p = 10^{13} \text{ Mpc}^{-1}$ . The solid lines

denote the results with the Gaussian window function, and the dashed lines represent those with the real-space top-hat window function. The required amplitude  $A$  of the primordial power spectrum is increasing along with the parameter  $\alpha$  and  $\beta$ . The reason is that the fraction of PBHs in the dark matter is the integration of mass function among the whole range as shown in equation (13), so a narrower peak in the primordial power spectrum requires a larger amplitude  $A$  to give the same fraction. A narrower peak is from a pair of larger  $\alpha$  and  $\beta$ , so the amplitude  $A$  increases along with the parameter  $\alpha$  and  $\beta$ . For the top-hat window function, the smallest value of the required amplitude is  $A \approx 3.24 \times 10^{-3}$ ; and for the Gaussian window function, it is  $A \approx 8.92 \times 10^{-3}$ , which is about three times larger than that with the top-hat window function. For the top-hat window function, the largest value of the required amplitude is  $A \approx 5.32 \times 10^{-3}$ ; and for the Gaussian window function, it is  $A \approx 1.51 \times 10^{-2}$ , which is also about three times larger than that with the top-hat window function. The largest value of  $A$  is around 1.7 times larger than the smallest value for each window function.

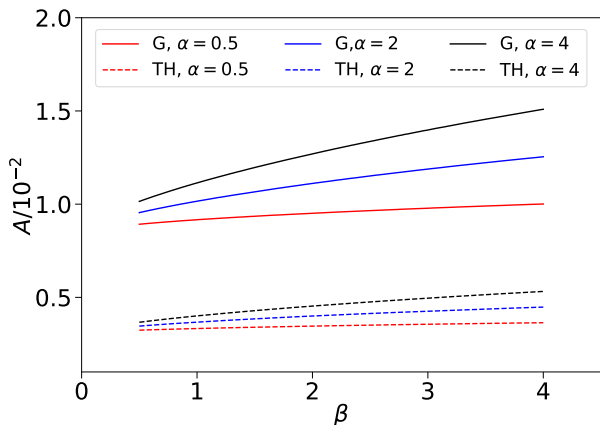


**Fig. 4** The required of amplitude  $A$  to explain all the dark matter. The solid and dashed lines are the results with the Gaussian and top-hat window functions, respectively.

For the case where PBHs explain all the dark matter, the corresponding SIGWs are displayed in figure 5. The black lines denote the energy density of SIGWs where the Gaussian window function is chosen to calculate the corresponding PBH mass function, and the red lines denote those with the top-hat window function being chosen. The dashed lines are the energy density of the GWs induced from the primordial power spectra with the broadest peak,  $\alpha = \beta = 0.5$ ; and the solid lines are from the primordial power spectra with the narrowest peak,  $\alpha = \beta = 4$ . If the PBHs formed from the primordial curvature perturbations can explain all the dark matter, the corresponding SIGWs will be detected by the future space-based GW detectors, and the profile of SIGWs

can determine the profile of the peak in the primordial curvature power spectrum. If the future space-based GW detectors do not detect the SIGWs, it indicates that the PBHs can only account for a part of dark matter.

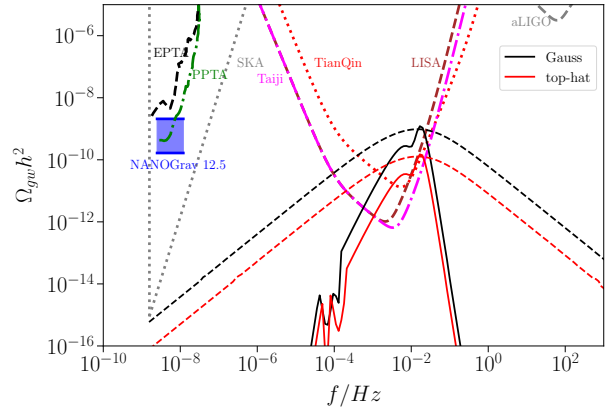


**Fig. 5** The convex curves denote the energy density of SIGWs, where the corresponding PBHs can explain all dark matter. The black and red curves represent the situations where the Gaussian window function and real-space top hat window function are chosen to calculate the corresponding PBH mass function, respectively. The dashed and solid lines are from the parameterization (32) with the broadest peak and the narrowest peak, respectively.

## 4.2 Constraints from SIGWs

The scalar-induced gravitational waves generated during the radiation domination are the components of the stochastic background of gravitational waves. The North American Nanohertz Observatory for Gravitational Wave (NANOGrav) Collaboration has published an analysis of the 12.5yrs pulsar timing array (PTA) data, where strong evidence of a stochastic process with a common amplitude and a common spectral slope across pulsars was found [115]. The same signal is also detected by other pulsar timing array groups [116, 117]. Although this process lacks quadrupolar spatial correlations, it is worth interpreting as a stochastic GW signal, which the SIGWs can explain with frequencies around  $10^{-9}$  Hz [58, 67, 118–120].

This paper constrains the power spectrum of the primordial curvature perturbation from the NANOGrav 12.5yrs data, assuming that the NANOGrav 12.5yrs signals are from SIGWs. We follow the analysis in ref. [158] and focus on the results of the NANOGrav free-spectrum analysis, where the signal in each frequency bin is fitted separately. Only the posteriors on the first five frequency bins are used due to the most constraining measurements coming at the lowest frequencies [115, 158]. The public data products are from <https://data.nanograv.org>. The log-likelihood function is obtained by evaluating the energy density of the SIGWs at

the five values  $f_i$  and summing the log probability density functions of the five independent kernel density estimates at these values [158]. The posteriors on the parameters of parameterization (32) are shown in figure 6, where the sampling is performed with the DYNesty [159] implementation of the nested sampling algorithm [160]; and the marginalized posterior distributions lead to the following mean values and one-sigma confidence intervals,

$$\log_{10} A = -1.95^{+0.37}_{-0.15}, \quad \log_{10} k = 6.04^{+0.29}_{-0.66}, \quad (33)$$

$$\alpha = 1.96^{+1.32}_{-1.08}, \quad \beta = 1.04^{+0.89}_{-0.38}. \quad (34)$$

By choosing these best parameter values (33) and (34), the power spectrum with the broken-power-law-parameterization (32) is displayed in the right panel of figure 2 and denoted by the black line. The corresponding mass function of PBHs calculated with peak theory and the Gaussian window function are shown in the left panel of figure 2 and represented by the black line, which are under the PBHs observational constraints. For the peak theory with the top-hat window function, the mass function at the peak is about  $f_{\text{PBH}}(M_{\text{PBH}}^{\text{peak}}) \sim 10^4$ , exceeding the PBHs observational constraints, which can also be understood from the right panel of figure 2, so we don't display them in the left panel of figure 2.

In figure 7, we take together the posteriors distribution from NANOGrav 12.5yrs data and other constraints on the primordial power spectrum. The blue regions are the  $1\sigma$  and  $2\sigma$  posteriors on the amplitude and scale, respectively. The orange and cyan regions are excluded by the BBN [152] and EPTA [151]. The black and red bands are the upper limits constrained from the PBHs observational data, as displayed in the right panel of figure 2.

## 5 Conclusion

The primordial black holes and scalar-induced gravitational waves can be produced from the large scalar perturbations in the early Universe. They can tell us information about the small-scale primordial curvature perturbation generated in the inflation. To form enough PBHs DM and induce detectable GWs, the amplitude of the primordial curvature power spectrum should be around  $\mathcal{P}_\zeta \sim \mathcal{O}(0.01)$ , which is about seven orders of magnitude larger than the constraints from CMB observational data at large scales. Generally, the enhanced region of the primordial power spectrum can be parameterized as the power law form. For the whole primordial power spectrum, we use the broken power law form to parameterize their profile, where the parameterization form is  $\mathcal{P}_\zeta(k) = A(\alpha + \beta)/[\beta(k/k_p)^{-\alpha} + \alpha(k/k_p)^\beta] + A_*(k/k_*)^{n_{s*}-1}$  with  $k_* = 0.05\text{Mpc}^{-1}$ ,  $n_{s*} = 0.965$ , and  $A_* = 2.1 \times 10^{-9}$ . The primordial curvature power spectrum with the broken power form can be produced from many inflation

models, such as nonminimal derivative coupling inflation, scalar-tensor inflation, Gauss-Bonnet inflation, and K/G inflation.

The fraction of PBHs in the dark matter is calculated by the peak theory, where both Gaussian and top-hat window functions are considered. With the help of the fraction equation, we obtain the constraints on the primordial curvature power spectrum from the present primary PBHs DM observational data. The results are displayed in the right panel of figure 2. For the choice of the top-hat window function, the constraints on the primordial curvature power spectrum from PBHs DM are more robust than those from BBN and EPTA. For the Gaussian window function, the constraints from PBHs DM are weaker than those from EPTA. The uncertainty of the constraints caused by the choice of the window function is more significant than that by the profile of the peak in the primordial curvature power spectrum; we should take care of the choice of the window function. Under the constraints of PBHs DM, the corresponding SIGWs with frequencies around  $10^{-9}$  Hz,  $10^{-3}$  Hz, and  $10^2$  Hz are shown in figure 3. The SIGWs with frequencies around  $10^{-9}$  Hz and  $10^{-3}$  Hz can be detected by PTA and the future space-based detectors, respectively. The SIGWs with frequencies around  $10^2$  Hz cannot be detected presently, and we will get little information about the early Universe from them. The required amplitudes of the primordial curvature power spectrum to explain all the dark matter are displayed in figure 4, and they depend on the shape of the spectrum peak and window function. For the top hat window function, to explain all the dark matter, the amplitude of the primordial power spectrum with the narrowest peak requires  $A \approx 5.32 \times 10^{-3}$  and  $A \approx 3.24 \times 10^{-2}$  with the broadest peak; for the Gaussian window function, it requires  $A \approx 1.51 \times 10^{-2}$  with the narrowest peak and  $A \approx 8.92 \times 10^{-3}$  with the broadest peak. The largest required amplitude is about 1.7 times larger than the smallest for each window function. The corresponding SIGWs can be detected by future space-based detectors, and the SIGWs can be used to verify whether PBHs can explain all the dark matter.

The constraints on the primordial curvature power spectrum from NANOGrav 12.5yrs data sets are displayed in figure 6 by assuming the NANOGrav signals are from SIGWs. The mean values and one-sigma confidence intervals of the broken power law parameterization of primordial curvature power spectrum obtained from the first five frequency bins of NANOGrav 12.5yrs data sets are  $\log_{10} A = -1.95^{+0.37}_{-0.15}$ ,  $\log_{10} k = 6.04^{+0.29}_{-0.66}$ ,  $\alpha = 1.96^{+1.32}_{-1.08}$ , and  $\beta = 1.04^{+0.89}_{-0.38}$ . The allowed region of the curvature power spectrum from the NANOGrav 12.5yrs data sets, the upper limits from the PBH observational data, and the excluded regions from BBN and EPTA are taken together in figure 7.

In conclusion, we give the constraints on the primordial curvature perturbations from the present primary PBHs ob-



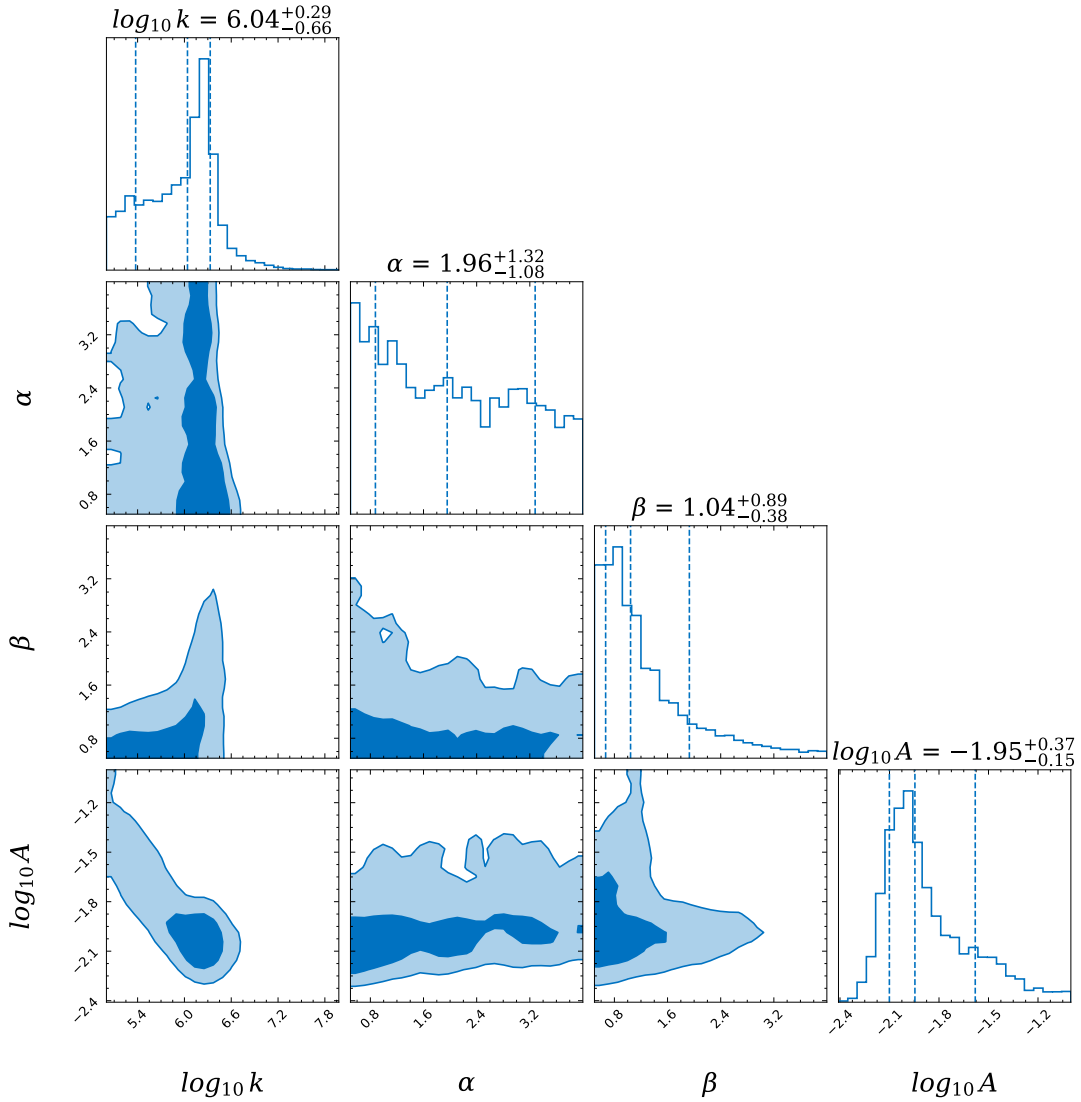


**Fig. 6** The posteriors on the parameters in parameterization (32) from the first five frequency bins of NANOGrav 12.5yrs data set, and the shaded areas denote  $1\sigma$  and  $2\sigma$  confidence regions.

servational data, where the fraction of PBHs in dark matter is calculated by the peak theory and the primordial curvature spectrum is parameterized by the broken power law form. The region of the primordial curvature spectrum to explain the NANOGrav 12.5yrs data sets is also obtained by assuming the NANOGrav signals are from SIGWs.

**Acknowledgements** We thank Xing-Jiang Zhu, Zu-Cheng Chen, Xiao-Jin Liu, Zhi-Qiang You, and Shen-Shi Du for useful discussions. This research is supported by the National Natural Science Foundation of China under Grant No. 12205015 and the supporting fund for young researcher of Beijing Normal University under Grant No. 28719/310432102.

## References

1. B.J. Carr, S.W. Hawking, Black holes in the early Universe, *Mon. Not. Roy. Astron. Soc.* **168**, 399 (1974)
2. S. Hawking, Gravitationally collapsed objects of very low mass, *Mon. Not. Roy. Astron. Soc.* **152**, 75 (1971)
3. S. Bird, I. Cholis, J.B. Muñoz, Y. Ali-Haïmoud, M. Kamionkowski, E.D. Kovetz, A. Raccanelli, A.G. Riess, Did LIGO detect dark matter?, *Phys. Rev. Lett.* **116**(20), 201301 (2016)
4. S. Clesse, J. García-Bellido, The clustering of massive Primordial Black Holes as Dark Matter: measuring their mass distribution with Advanced LIGO, *Phys. Dark Univ.* **15**, 142 (2017)
5. M. Sasaki, T. Suyama, T. Tanaka, S. Yokoyama, Primordial Black Hole Scenario for the Gravitational-

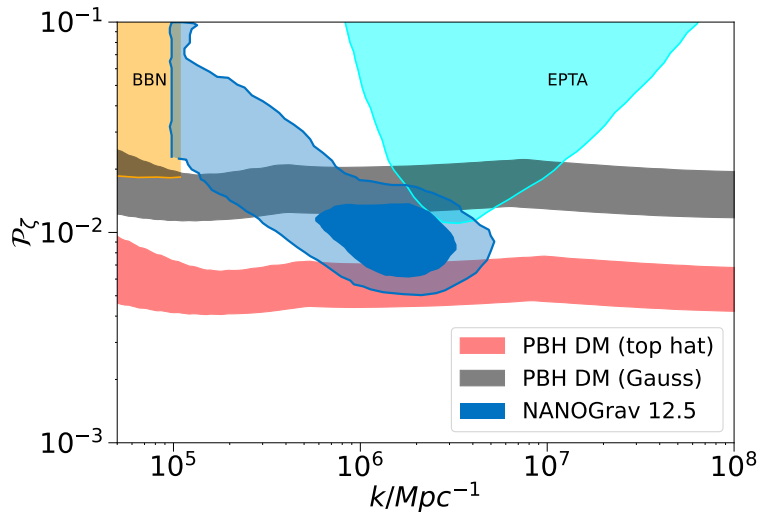


**Fig. 7** The constraints on the primordial curvature power spectrum. The orange and cyan regions are excluded by BBN [152] and EPTA [151]. The blue area is the allowed region to explain the NANOGrav 12.5 yrs data sets; the two contours denote the  $1\sigma$  and  $2\sigma$  confidence regions, respectively. The black and red bands are the upper limits constrained from the PBHs observational data, as displayed in the right panel of figure 2.

- Wave Event GW150914, Phys. Rev. Lett. **117**(6), 061101 (2016). [Erratum: Phys.Rev.Lett. 121, 059901 (2018)]
6. B.P. Abbott, et al., Observation of Gravitational Waves from a Binary Black Hole Merger, Phys. Rev. Lett. **116**(6), 061102 (2016)
  7. B.P. Abbott, et al., GW151226: Observation of Gravitational Waves from a 22-Solar-Mass Binary Black Hole Coalescence, Phys. Rev. Lett. **116**(24), 241103 (2016)
  8. B.P. Abbott, et al., GW170104: Observation of a 50-Solar-Mass Binary Black Hole Coalescence at Redshift 0.2, Phys. Rev. Lett. **118**(22), 221101 (2017). [Erratum: Phys.Rev.Lett. 121, 129901 (2018)]
  9. B.P. Abbott, et al., GW170814: A Three-Detector Observation of Gravitational Waves from a Binary Black Hole Coalescence, Phys. Rev. Lett. **119**(14), 141101 (2017)
  10. B.P. Abbott, et al., GW170817: Observation of Gravitational Waves from a Binary Neutron Star Inspiral, Phys. Rev. Lett. **119**(16), 161101 (2017)
  11. B.P. Abbott, et al., GW170608: Observation of a 19-solar-mass Binary Black Hole Coalescence, Astrophys. J. Lett. **851**, L35 (2017)
  12. B.P. Abbott, et al., GWTC-1: A Gravitational-Wave Transient Catalog of Compact Binary Mergers Observed by LIGO and Virgo during the First and Second Observing Runs, Phys. Rev. X **9**(3), 031040 (2019)
  13. B.P. Abbott, et al., GW190425: Observation of a Compact Binary Coalescence with Total Mass  $\sim 3.4M_{\odot}$ , Astrophys. J. Lett. **892**(1), L3 (2020)
  14. R. Abbott, et al., GW190412: Observation of a Binary-Black-Hole Coalescence with Asymmetric Masses, Phys. Rev. D **102**(4), 043015 (2020)
  15. R. Abbott, et al., GW190814: Gravitational Waves from the Coalescence of a 23 Solar Mass Black Hole with a 2.6 Solar Mass Compact Object, Astrophys. J. Lett. **896**(2), L44 (2020)
  16. R. Abbott, et al., GW190521: A Binary Black Hole Merger with a Total Mass of  $150M_{\odot}$ , Phys. Rev. Lett. **125**(10), 101102 (2020)
  17. R. Abbott, et al., GWTC-2: Compact Binary Coalescences Observed by LIGO and Virgo During the First Half of the Third Observing Run, Phys. Rev. X **11**, 021053 (2021)
  18. P. Ivanov, P. Naselsky, I. Novikov, Inflation and primordial black holes as dark matter, Phys. Rev. D **50**, 7173 (1994)
  19. P.H. Frampton, M. Kawasaki, F. Takahashi, T.T. Yanagida, Primordial Black Holes as All Dark Matter, JCAP **04**, 023 (2010)
  20. K.M. Belotsky, A.D. Dmitriev, E.A. Esipova, V.A. Gani, A.V. Grobov, M.Y. Khlopov, A.A. Kirillov, S.G. Rubin, I.V. Svadkovsky, Signatures of primordial black hole dark matter, Mod. Phys. Lett. A **29**(37), 1440005 (2014)
  21. M.Y. Khlopov, S.G. Rubin, A.S. Sakharov, Primordial structure of massive black hole clusters, Astropart. Phys. **23**, 265 (2005)
  22. S. Clesse, J. García-Bellido, Massive Primordial Black Holes from Hybrid Inflation as Dark Matter and the seeds of Galaxies, Phys. Rev. D **92**(2), 023524 (2015)

23. B. Carr, F. Kuhnel, M. Sandstad, Primordial Black Holes as Dark Matter, *Phys. Rev. D* **94**(8), 083504 (2016)
24. K. Inomata, M. Kawasaki, K. Mukaida, Y. Tada, T.T. Yanagida, Inflationary Primordial Black Holes as All Dark Matter, *Phys. Rev. D* **96**(4), 043504 (2017)
25. J. García-Bellido, Massive Primordial Black Holes as Dark Matter and their detection with Gravitational Waves, *J. Phys. Conf. Ser.* **840**(1), 012032 (2017)
26. E.D. Kovetz, Probing Primordial-Black-Hole Dark Matter with Gravitational Waves, *Phys. Rev. Lett.* **119**(13), 131301 (2017)
27. B. Carr, F. Kuhnel, Primordial Black Holes as Dark Matter: Recent Developments, *Ann. Rev. Nucl. Part. Sci.* **70**, 355 (2020)
28. A.H. Guth, The Inflationary Universe: A Possible Solution to the Horizon and Flatness Problems, *Phys. Rev. D* **23**, 347 (1981)
29. A.D. Linde, A New Inflationary Universe Scenario: A Possible Solution of the Horizon, Flatness, Homogeneity, Isotropy and Primordial Monopole Problems, *Phys. Lett. B* **108**, 389 (1982)
30. A. Albrecht, P.J. Steinhardt, Cosmology for Grand Unified Theories with Radiatively Induced Symmetry Breaking, *Phys. Rev. Lett.* **48**, 1220 (1982)
31. A.A. Starobinsky, A New Type of Isotropic Cosmological Models Without Singularity, *Phys. Lett. B* **91**, 99 (1980)
32. Y. Akrami, et al., Planck 2018 results. X. Constraints on inflation, *Astron. Astrophys.* **641**, A10 (2020)
33. H. Di, Y. Gong, Primordial black holes and second order gravitational waves from ultra-slow-roll inflation, *JCAP* **07**, 007 (2018)
34. J. Martin, H. Motohashi, T. Suyama, Ultra Slow-Roll Inflation and the non-Gaussianity Consistency Relation, *Phys. Rev. D* **87**(2), 023514 (2013)
35. H. Motohashi, A.A. Starobinsky, J. Yokoyama, Inflation with a constant rate of roll, *JCAP* **09**, 018 (2015)
36. Z. Yi, Y. Gong, On the constant-roll inflation, *JCAP* **03**, 052 (2018)
37. J. Garcia-Bellido, E. Ruiz Morales, Primordial black holes from single field models of inflation, *Phys. Dark Univ.* **18**, 47 (2017)
38. C. Germani, T. Prokopec, On primordial black holes from an inflection point, *Phys. Dark Univ.* **18**, 6 (2017)
39. H. Motohashi, W. Hu, Primordial Black Holes and Slow-Roll Violation, *Phys. Rev. D* **96**(6), 063503 (2017)
40. J.M. Ezquiaga, J. Garcia-Bellido, E. Ruiz Morales, Primordial Black Hole production in Critical Higgs Inflation, *Phys. Lett. B* **776**, 345 (2018)
41. G. Ballesteros, J. Beltran Jimenez, M. Pieroni, Black hole formation from a general quadratic action for inflationary primordial fluctuations, *JCAP* **06**, 016 (2019)
42. I. Dalianis, A. Kehagias, G. Tringas, Primordial black holes from  $\alpha$ -attractors, *JCAP* **01**, 037 (2019)
43. F. Bezrukov, M. Pauly, J. Rubio, On the robustness of the primordial power spectrum in renormalized Higgs inflation, *JCAP* **02**, 040 (2018)
44. S. Passaglia, W. Hu, H. Motohashi, Primordial black holes and local non-Gaussianity in canonical inflation, *Phys. Rev. D* **99**(4), 043536 (2019)
45. A.Y. Kamenshchik, A. Tronconi, T. Vardanyan, G. Venturi, Non-Canonical Inflation and Primordial Black Holes Production, *Phys. Lett. B* **791**, 201 (2019)
46. C. Fu, P. Wu, H. Yu, Primordial Black Holes from Inflation with Nonminimal Derivative Coupling, *Phys. Rev. D* **100**(6), 063532 (2019)
47. C. Fu, P. Wu, H. Yu, Scalar induced gravitational waves in inflation with gravitationally enhanced friction, *Phys. Rev. D* **101**(2), 023529 (2020)
48. I. Dalianis, S. Karydas, E. Papantonopoulos, Generalized Non-Minimal Derivative Coupling: Application to Inflation and Primordial Black Hole Production, *JCAP* **06**, 040 (2020)
49. M. Braglia, D.K. Hazra, F. Finelli, G.F. Smoot, L. Sriramkumar, A.A. Starobinsky, Generating PBHs and small-scale GWs in two-field models of inflation, *JCAP* **08**, 001 (2020)
50. A. Gundhi, C.F. Steinwachs, Scalaron–Higgs inflation reloaded: Higgs-dependent scalaron mass and primordial black hole dark matter, *Eur. Phys. J. C* **81**(5), 460 (2021)
51. D.Y. Cheong, S.M. Lee, S.C. Park, Primordial black holes in Higgs- $R^2$  inflation as the whole of dark matter, *JCAP* **01**, 032 (2021)
52. J. Lin, Q. Gao, Y. Gong, Y. Lu, C. Zhang, F. Zhang, Primordial black holes and secondary gravitational waves from  $k$  and  $G$  inflation, *Phys. Rev. D* **101**(10), 103515 (2020)
53. J. Lin, S. Gao, Y. Gong, Y. Lu, Z. Wang, F. Zhang, Primordial black holes and scalar induced secondary gravitational waves from Higgs inflation with non-canonical kinetic term, arXiv: 2111.01362, (2021)
54. Q. Gao, Y. Gong, Z. Yi, Primordial black holes and secondary gravitational waves from natural inflation, *Nucl. Phys. B* **969**, 115480 (2021)
55. Q. Gao, Primordial black holes and secondary gravitational waves from chaotic inflation, *Sci. China Phys. Mech. Astron.* **64**(8), 280411 (2021)
56. Z. Yi, Y. Gong, B. Wang, Z.h. Zhu, Primordial black holes and secondary gravitational waves from the Higgs field, *Phys. Rev. D* **103**(6), 063535 (2021)
57. Z. Yi, Q. Gao, Y. Gong, Z.h. Zhu, Primordial black holes and scalar-induced secondary gravitational

- waves from inflationary models with a noncanonical kinetic term, *Phys. Rev. D* **103**(6), 063534 (2021)
58. Z. Yi, Z.H. Zhu, NANOGrav signal and LIGO-Virgo primordial black holes from the Higgs field, *JCAP* **05**(05), 046 (2022)
  59. Z. Yi, Primordial black holes and scalar-induced gravitational waves from scalar-tensor inflation, arXiv: 2206.01039, (2022)
  60. F. Zhang, Primordial black holes and scalar induced gravitational waves from the E model with a Gauss-Bonnet term, *Phys. Rev. D* **105**(6), 063539 (2022)
  61. S. Kawai, J. Kim, Primordial black holes from Gauss-Bonnet-corrected single field inflation, *Phys. Rev. D* **104**(8), 083545 (2021)
  62. R.G. Cai, C. Chen, C. Fu, Primordial black holes and stochastic gravitational wave background from inflation with a noncanonical spectator field, *Phys. Rev. D* **104**(8), 083537 (2021)
  63. P. Chen, S. Koh, G. Tumurtushaa, Primordial black holes and induced gravitational waves from inflation in the Horndeski theory of gravity, arXiv: 2107.08638, (2021)
  64. R. Zheng, J. Shi, T. Qiu, On primordial black holes and secondary gravitational waves generated from inflation with solo/multi-bumpy potential \*, *Chin. Phys. C* **46**(4), 045103 (2022)
  65. C.T. Byrnes, P.S. Cole, S.P. Patil, Steepest growth of the power spectrum and primordial black holes, *JCAP* **06**, 028 (2019)
  66. P. Carrilho, K.A. Malik, D.J. Mulryne, Dissecting the growth of the power spectrum for primordial black holes, *Phys. Rev. D* **100**(10), 103529 (2019)
  67. V. Vaskonen, H. Veermäe, Did NANOGrav see a signal from primordial black hole formation?, *Phys. Rev. Lett.* **126**(5), 051303 (2021)
  68. G. Sato-Polito, E.D. Kovetz, M. Kamionkowski, Constraints on the primordial curvature power spectrum from primordial black holes, *Phys. Rev. D* **100**(6), 063521 (2019)
  69. A. Kalaja, N. Bellomo, N. Bartolo, D. Bertacca, S. Matarrese, I. Musco, A. Raccanelli, L. Verde, From Primordial Black Holes Abundance to Primordial Curvature Power Spectrum (and back), *JCAP* **10**, 031 (2019)
  70. A.D. Gow, C.T. Byrnes, P.S. Cole, S. Young, The power spectrum on small scales: Robust constraints and comparing PBH methodologies, *JCAP* **02**, 002 (2021)
  71. S. Matarrese, S. Mollerach, M. Bruni, Second order perturbations of the Einstein-de Sitter universe, *Phys. Rev. D* **58**, 043504 (1998)
  72. S. Mollerach, D. Harari, S. Matarrese, CMB polarization from secondary vector and tensor modes, *Phys. Rev. D* **69**, 063002 (2004)
  73. K.N. Ananda, C. Clarkson, D. Wands, The Cosmological gravitational wave background from primordial density perturbations, *Phys. Rev. D* **75**, 123518 (2007)
  74. D. Baumann, P.J. Steinhardt, K. Takahashi, K. Ichiki, Gravitational Wave Spectrum Induced by Primordial Scalar Perturbations, *Phys. Rev. D* **76**, 084019 (2007)
  75. J. Garcia-Bellido, M. Peloso, C. Unal, Gravitational Wave signatures of inflationary models from Primordial Black Hole Dark Matter, *JCAP* **09**, 013 (2017)
  76. R. Saito, J. Yokoyama, Gravitational wave background as a probe of the primordial black hole abundance, *Phys. Rev. Lett.* **102**, 161101 (2009). [Erratum: *Phys.Rev.Lett.* 107, 069901 (2011)]
  77. R. Saito, J. Yokoyama, Gravitational-Wave Constraints on the Abundance of Primordial Black Holes, *Prog. Theor. Phys.* **123**, 867 (2010). [Erratum: *Prog.Theor.Phys.* 126, 351–352 (2011)]
  78. E. Bugaev, P. Klimai, Induced gravitational wave background and primordial black holes, *Phys. Rev. D* **81**, 023517 (2010)
  79. E. Bugaev, P. Klimai, Constraints on the induced gravitational wave background from primordial black holes, *Phys. Rev. D* **83**, 083521 (2011)
  80. L. Alabidi, K. Kohri, M. Sasaki, Y. Sendouda, Observable Spectra of Induced Gravitational Waves from Inflation, *JCAP* **09**, 017 (2012)
  81. N. Orlofsky, A. Pierce, J.D. Wells, Inflationary theory and pulsar timing investigations of primordial black holes and gravitational waves, *Phys. Rev. D* **95**(6), 063518 (2017)
  82. T. Nakama, J. Silk, M. Kamionkowski, Stochastic gravitational waves associated with the formation of primordial black holes, *Phys. Rev. D* **95**(4), 043511 (2017)
  83. K. Inomata, M. Kawasaki, K. Mukaida, Y. Tada, T.T. Yanagida, Inflationary primordial black holes for the LIGO gravitational wave events and pulsar timing array experiments, *Phys. Rev. D* **95**(12), 123510 (2017)
  84. S.L. Cheng, W. Lee, K.W. Ng, Primordial black holes and associated gravitational waves in axion monodromy inflation, *JCAP* **07**, 001 (2018)
  85. R.g. Cai, S. Pi, M. Sasaki, Gravitational Waves Induced by non-Gaussian Scalar Perturbations, *Phys. Rev. Lett.* **122**(20), 201101 (2019)
  86. N. Bartolo, V. De Luca, G. Franciolini, M. Peloso, D. Racco, A. Riotto, Testing primordial black holes as dark matter with LISA, *Phys. Rev. D* **99**(10), 103521 (2019)
  87. N. Bartolo, V. De Luca, G. Franciolini, A. Lewis, M. Peloso, A. Riotto, Primordial Black Hole Dark Matter: LISA Serendipity, *Phys. Rev. Lett.* **122**(21), 211301 (2019)

88. K. Kohri, T. Terada, Semianalytic calculation of gravitational wave spectrum nonlinearly induced from primordial curvature perturbations, *Phys. Rev. D* **97**(12), 123532 (2018)
89. J.R. Espinosa, D. Racco, A. Riotto, A Cosmological Signature of the SM Higgs Instability: Gravitational Waves, *JCAP* **09**, 012 (2018)
90. R.G. Cai, S. Pi, S.J. Wang, X.Y. Yang, Resonant multiple peaks in the induced gravitational waves, *JCAP* **05**, 013 (2019)
91. R.G. Cai, S. Pi, S.J. Wang, X.Y. Yang, Pulsar Timing Array Constraints on the Induced Gravitational Waves, *JCAP* **10**, 059 (2019)
92. R.G. Cai, Z.K. Guo, J. Liu, L. Liu, X.Y. Yang, Primordial black holes and gravitational waves from parametric amplification of curvature perturbations, *JCAP* **06**, 013 (2020)
93. R.G. Cai, Y.C. Ding, X.Y. Yang, Y.F. Zhou, Constraints on a mixed model of dark matter particles and primordial black holes from the galactic 511 keV line, *JCAP* **03**, 057 (2021)
94. G. Domènech, Induced gravitational waves in a general cosmological background, *Int. J. Mod. Phys. D* **29**(03), 2050028 (2020)
95. G. Domènech, S. Pi, M. Sasaki, Induced gravitational waves as a probe of thermal history of the universe, *JCAP* **08**, 017 (2020)
96. J. Fumagalli, S. Renaux-Petel, J.W. Ronayne, L.T. Witkowski, Turning in the landscape: a new mechanism for generating Primordial Black Holes, arXiv: 2004.08369 (2020)
97. J. Fumagalli, S. Renaux-Petel, L.T. Witkowski, Oscillations in the stochastic gravitational wave background from sharp features and particle production during inflation, *JCAP* **08**, 030 (2021)
98. A. Ashoorioon, K. Rezazadeh, A. Rostami, NANOGrav signal from the end of inflation and the LIGO mass and heavier primordial black holes, *Phys. Lett. B* **835**, 137542 (2022)
99. S. Pi, M. Sasaki, Gravitational Waves Induced by Scalar Perturbations with a Lognormal Peak, *JCAP* **09**, 037 (2020)
100. C. Yuan, Z.C. Chen, Q.G. Huang, Scalar induced gravitational waves in different gauges, *Phys. Rev. D* **101**(6), 063018 (2020)
101. C. Yuan, Z.C. Chen, Q.G. Huang, Log-dependent slope of scalar induced gravitational waves in the infrared regions, *Phys. Rev. D* **101**(4), 043019 (2020)
102. C. Yuan, Z.C. Chen, Q.G. Huang, Probing primordial–black-hole dark matter with scalar induced gravitational waves, *Phys. Rev. D* **100**(8), 081301 (2019)
103. T. Papanikolaou, V. Vennin, D. Langlois, Gravitational waves from a universe filled with primordial black holes, *JCAP* **03**, 053 (2021)
104. T. Papanikolaou, C. Tzerefos, S. Basilakos, E.N. Saridakis, Scalar induced gravitational waves from primordial black hole Poisson fluctuations in  $f(R)$  gravity, *JCAP* **10**, 013 (2022)
105. T. Papanikolaou, C. Tzerefos, S. Basilakos, E.N. Saridakis, No constraints for  $f(T)$  gravity from gravitational waves induced from primordial black hole fluctuations (2022)
106. R.D. Ferdman, et al., The European Pulsar Timing Array: current efforts and a LEAP toward the future, *Class. Quant. Grav.* **27**, 084014 (2010)
107. G. Hobbs, et al., The international pulsar timing array project: using pulsars as a gravitational wave detector, *Class. Quant. Grav.* **27**, 084013 (2010)
108. M.A. McLaughlin, The North American Nanohertz Observatory for Gravitational Waves, *Class. Quant. Grav.* **30**, 224008 (2013)
109. G. Hobbs, The Parkes Pulsar Timing Array, *Class. Quant. Grav.* **30**, 224007 (2013)
110. C.J. Moore, R.H. Cole, C.P.L. Berry, Gravitational-wave sensitivity curves, *Class. Quant. Grav.* **32**(1), 015014 (2015)
111. K. Danzmann, LISA: An ESA cornerstone mission for a gravitational wave observatory, *Class. Quant. Grav.* **14**, 1399 (1997)
112. P. Amaro-Seoane, et al., Laser Interferometer Space Antenna, arXiv: 1702.00786, (2017)
113. W.R. Hu, Y.L. Wu, The Taiji Program in Space for gravitational wave physics and the nature of gravity, *Natl. Sci. Rev.* **4**(5), 685 (2017)
114. J. Luo, et al., TianQin: a space-borne gravitational wave detector, *Class. Quant. Grav.* **33**(3), 035010 (2016)
115. Z. Arzoumanian, et al., The NANOGrav 12.5 yr Data Set: Search for an Isotropic Stochastic Gravitational-wave Background, *Astrophys. J. Lett.* **905**(2), L34 (2020)
116. B. Goncharov, et al., On the Evidence for a Common-spectrum Process in the Search for the Nanohertz Gravitational-wave Background with the Parkes Pulsar Timing Array, *Astrophys. J. Lett.* **917**(2), L19 (2021)
117. J. Antoniadis, et al., The International Pulsar Timing Array second data release: Search for an isotropic gravitational wave background, *Mon. Not. Roy. Astron. Soc.* **510**(4), 4873 (2022)
118. V. De Luca, G. Franciolini, A. Riotto, NANOGrav Data Hints at Primordial Black Holes as Dark Matter, *Phys. Rev. Lett.* **126**(4), 041303 (2021)
119. K. Inomata, M. Kawasaki, K. Mukaida, T.T. Yanagida, NANOGrav Results and LIGO-Virgo Primordial

- Black Holes in Axionlike Curvaton Models, *Phys. Rev. Lett.* **126**(13), 131301 (2021)
120. G. Domènech, S. Pi, NANOGrav hints on planet-mass primordial black holes, *Sci. China Phys. Mech. Astron.* **65**(3), 230411 (2022)
  121. J.M. Bardeen, J.R. Bond, N. Kaiser, A.S. Szalay, The Statistics of Peaks of Gaussian Random Fields, *Astrophys. J.* **304**, 15 (1986)
  122. A.M. Green, A.R. Liddle, K.A. Malik, M. Sasaki, A New calculation of the mass fraction of primordial black holes, *Phys. Rev. D* **70**, 041502 (2004)
  123. S. Young, C.T. Byrnes, M. Sasaki, Calculating the mass fraction of primordial black holes, *JCAP* **07**, 045 (2014)
  124. C. Germani, I. Musco, Abundance of Primordial Black Holes Depends on the Shape of the Inflationary Power Spectrum, *Phys. Rev. Lett.* **122**(14), 141302 (2019)
  125. S. Young, M. Musso, Application of peaks theory to the abundance of primordial black holes, *JCAP* **11**, 022 (2020)
  126. K. Ando, K. Inomata, M. Kawasaki, Primordial black holes and uncertainties in the choice of the window function, *Phys. Rev. D* **97**(10), 103528 (2018)
  127. M.W. Choptuik, Universality and scaling in gravitational collapse of a massless scalar field, *Phys. Rev. Lett.* **70**, 9 (1993)
  128. C.R. Evans, J.S. Coleman, Observation of critical phenomena and selfsimilarity in the gravitational collapse of radiation fluid, *Phys. Rev. Lett.* **72**, 1782 (1994)
  129. J.C. Niemeyer, K. Jedamzik, Near-critical gravitational collapse and the initial mass function of primordial black holes, *Phys. Rev. Lett.* **80**, 5481 (1998)
  130. S. Young, The primordial black hole formation criterion re-examined: Parametrisation, timing and the choice of window function, *Int. J. Mod. Phys. D* **29**(02), 2030002 (2019)
  131. I. Musco, Threshold for primordial black holes: Dependence on the shape of the cosmological perturbations, *Phys. Rev. D* **100**(12), 123524 (2019)
  132. C.T. Byrnes, M. Hindmarsh, S. Young, M.R.S. Hawkins, Primordial black holes with an accurate QCD equation of state, *JCAP* **08**, 041 (2018)
  133. Y. Lu, Y. Gong, Z. Yi, F. Zhang, Constraints on primordial curvature perturbations from primordial black hole dark matter and secondary gravitational waves, *JCAP* **12**, 031 (2019)
  134. Y. Akrami, et al., Planck 2018 results. X. Constraints on inflation, *Astron. Astrophys.* **641**, A10 (2020)
  135. Y. Ali-Haïmoud, M. Kamionkowski, Cosmic microwave background limits on accreting primordial black holes, *Phys. Rev. D* **95**(4), 043534 (2017)
  136. V. Poulin, P.D. Serpico, F. Calore, S. Clesse, K. Kohri, CMB bounds on disk-accreting massive primordial black holes, *Phys. Rev. D* **96**(8), 083524 (2017)
  137. Y. Ali-Haïmoud, E.D. Kovetz, M. Kamionkowski, Merger rate of primordial black-hole binaries, *Phys. Rev. D* **96**(12), 123523 (2017)
  138. M. Raidal, C. Spethmann, V. Vaskonen, H. Veermäe, Formation and Evolution of Primordial Black Hole Binaries in the Early Universe, *JCAP* **02**, 018 (2019)
  139. V. Vaskonen, H. Veermäe, Lower bound on the primordial black hole merger rate, *Phys. Rev. D* **101**(4), 043015 (2020)
  140. V. De Luca, G. Franciolini, P. Pani, A. Riotto, Primordial Black Holes Confront LIGO/Virgo data: Current situation, *JCAP* **06**, 044 (2020)
  141. K.W.K. Wong, G. Franciolini, V. De Luca, V. Baibhav, E. Berti, P. Pani, A. Riotto, Constraining the primordial black hole scenario with Bayesian inference and machine learning: the GWTC-2 gravitational wave catalog, *Phys. Rev. D* **103**(2), 023026 (2021)
  142. G. Hütsi, M. Raidal, V. Vaskonen, H. Veermäe, Two populations of LIGO-Virgo black holes, *JCAP* **03**, 068 (2021)
  143. P. Tisserand, et al., Limits on the Macho Content of the Galactic Halo from the EROS-2 Survey of the Magellanic Clouds, *Astron. Astrophys.* **469**, 387 (2007)
  144. H. Niikura, et al., Microlensing constraints on primordial black holes with Subaru/HSC Andromeda observations, *Nature Astron.* **3**(6), 524 (2019)
  145. K. Griest, A.M. Cieplak, M.J. Lehner, New Limits on Primordial Black Hole Dark Matter from an Analysis of Kepler Source Microlensing Data, *Phys. Rev. Lett.* **111**(18), 181302 (2013)
  146. P.W. Graham, S. Rajendran, J. Varela, Dark Matter Triggers of Supernovae, *Phys. Rev. D* **92**(6), 063007 (2015)
  147. R. Laha, Primordial Black Holes as a Dark Matter Candidate Are Severely Constrained by the Galactic Center 511 keV  $\gamma$ -Ray Line, *Phys. Rev. Lett.* **123**(25), 251101 (2019)
  148. B. Dasgupta, R. Laha, A. Ray, Neutrino and positron constraints on spinning primordial black hole dark matter, *Phys. Rev. Lett.* **125**(10), 101101 (2020)
  149. R. Laha, J.B. Muñoz, T.R. Slatyer, INTEGRAL constraints on primordial black holes and particle dark matter, *Phys. Rev. D* **101**(12), 123514 (2020)
  150. B.J. Carr, K. Kohri, Y. Sendouda, J. Yokoyama, New cosmological constraints on primordial black holes, *Phys. Rev. D* **81**, 104019 (2010)
  151. K. Inomata, T. Nakama, Gravitational waves induced by scalar perturbations as probes of the small-scale primordial spectrum, *Phys. Rev. D* **99**(4), 043511 (2019)
  152. K. Inomata, M. Kawasaki, Y. Tada, Revisiting constraints on small scale perturbations from big-bang nucleosynthesis, *Phys. Rev. D* **94**(4), 043527 (2016)

- 
153. D.J. Fixsen, E.S. Cheng, J.M. Gales, J.C. Mather, R.A. Shafer, E.L. Wright, The Cosmic Microwave Background spectrum from the full COBE FIRAS data set, *Astrophys. J.* **473**, 576 (1996)
  154. L. Lentati, et al., European Pulsar Timing Array Limits On An Isotropic Stochastic Gravitational-Wave Background, *Mon. Not. Roy. Astron. Soc.* **453**(3), 2576 (2015)
  155. R.M. Shannon, et al., Gravitational waves from binary supermassive black holes missing in pulsar observations, *Science* **349**(6255), 1522 (2015)
  156. G.M. Harry, Advanced LIGO: The next generation of gravitational wave detectors, *Class. Quant. Grav.* **27**, 084006 (2010)
  157. J. Aasi, et al., Advanced LIGO, *Class. Quant. Grav.* **32**, 074001 (2015)
  158. C.J. Moore, A. Vecchio, Ultra-low-frequency gravitational waves from cosmological and astrophysical processes, *Nature Astron.* **5**(12), 1268 (2021)
  159. J.S. Speagle, dynesty: a dynamic nested sampling package for estimating Bayesian posteriors and evidences, *Mon. Not. Roy. Astron. Soc.* **493**(3), 3132 (2020)
  160. J. Skilling, Nested Sampling, *AIP Conf. Proc.* **735**, 395 (2004)